

Multivariable lateral control of an off-road vehicle operating on sloping grounds

Romain Legrand, Fabien Claveau, Philippe Chevrel, Benjamin Rancinangue, Anthony Dollet

▶ **To cite this version:**

Romain Legrand, Fabien Claveau, Philippe Chevrel, Benjamin Rancinangue, Anthony Dollet. Multivariable lateral control of an off-road vehicle operating on sloping grounds. ECC 2022: European Control Conference, Jul 2022, London, United Kingdom. 10.23919/ECC55457.2022.9838119 . hal-03631799

HAL Id: hal-03631799
https://hal.science/hal-03631799

Submitted on 5 Apr 2022

HAL is a multi-disciplinary open access archive for the deposit and dissemination of scientific research documents, whether they are published or not. The documents may come from teaching and research institutions in France or abroad, or from public or private research centers.

L'archive ouverte pluridisciplinaire **HAL**, est destinée au dépôt et à la diffusion de documents scientifiques de niveau recherche, publiés ou non, émanant des établissements d'enseignement et de recherche français ou étrangers, des laboratoires publics ou privés.

Multivariable lateral control of an off-road vehicle operating on sloping grounds

Romain Legrand, Fabien Claveau, Philippe Chevrel, Benjamin Rancinangue, Anthony Dollet

***Abstract*—This paper proposes an optimized lateral control design of a two-steering-axle off-road vehicle. An extension of the well-known bicycle model is introduced that considers two steering axles and the slope of the local ground. Lateral deviation controllers are thereby synthesized to quantitatively evaluate the use of multiple steering angles. The proposed multi-input multi-output feedback controllers originate from a H2/Hinf multi-objective synthesis, achieving optimum trade-offs between performance and robustness. Three controller architectures are considered (depending on actuation possibilities) and compared qualitatively and quantitatively. In addition, realistic simulation results are analyzed using a non-linear simulator that considers the fine modeling of sensors and actuators (e.g., hydraulic actuator). The results are promising and will be the subject of an experimental validation project.**

***Index Terms*—unmanned autonomous vehicles, autonomous vehicles, robust control, H infinity control, motion control**

I. Introduction

Autonomous vehicle research represents a dynamic and revolutionary area of robotics. It arose some decades ago [1] and grew rapidly in the on-road context [2], to the point where autonomous transport vehicles approach market availability. Off-road vehicles are included in this trend and have represented an interesting topic for more than two decades [3], despite numerous constraints such as the lack of grip or important slopes that are traditionally ignored in on-road path-following research. In addition, localization improvements due to more reliable GPS satellite constellations and easier access to high-capacity embedded computers have allowed breakthroughs in off-road autonomous vehicle research.

On-road vehicle research regards high speeds and traditionally adopted dynamic models based on the well-known bicycle model [4], [5], [6], [7] while off-road research, notably due to high slips, prefers to adopt a robotic perspective by widely considering kinematic or extended kinematic models [8], [9]. Off-road works are nonetheless beginning to consider dynamic models [10], demonstrating a convergence between the two fields.

Off-road vehicles are more likely to have two steerable axles or even four independent steerable wheels to perform complex maneuvers. Studies on two-axle vehicles often focus on a slip-free context that considers indoor vehicles [11]. Although non-slip hypothesis is widely assumed in this literature, the extended kinematic model enables considering the slip of the vehicle in the off-road context. [12]. The dynamic bicycle model also considers the slip of the vehicle, even when both front and rear wheels are steerable [13].

Some studies seek to estimate the slopes (lateral and/or longitudinal) in a safety context [14] to reduce rollover risks, but these estimations are rarely used in the feedback loop.

Our objective is to design a longitudinal and lateral regulation system dedicated to an autonomous off-road vehicle that may have two steering axles and may be subject to high slips due to the context of use (slippery soil, high slopes). This paper focuses on lateral control involving a two-steering-axle bicycle model able to predict slips at the front and rear pneumatics. This model will be usefull within the multivariable H_2/H_∞ control strategies known to efficiently manage performance-robustness trade-offs. Such strategies have proven their effectiveness for on-road vehicles at an experimental level [15], [16]and thus constitute a promising method of controlling two steering axles in a cooperative manner for off-road vehicles as well. The regulation system comprises two mains parts : The first is a feedforward component using knowledge of the lateral slope and curvature for a prior estimation of the steering angles to apply to the vehicle; the second is a feedback action exploiting lateral and angular deviations. The cornering stiffness of the wheels and location of the center of gravity should be estimated for this dynamic model-based controller to function.

This paper is organized as follows: first, the extended lateral linear vehicle model is presented with two steering axles and the lateral slope angle; the second part focuses on the multi-objective control design; and finally, the control solution is tested using a non-linear realistic simulator.

II. Two-steering-axle bicycle model on a sloping ground

The model shown in Fig. 1 is intended to support the lateral control design process of a vehicle with one steering axle (1SA) or two steering axles (2SA). This model must be simple enough for use and precise enough to allow generating *ad hoc* control laws parameterized by the longitudinal speed v_x. In the context of this paper, the traditional bicycle model must be enriched to represent the cases of 1SA and 2SA vehicle while considering the

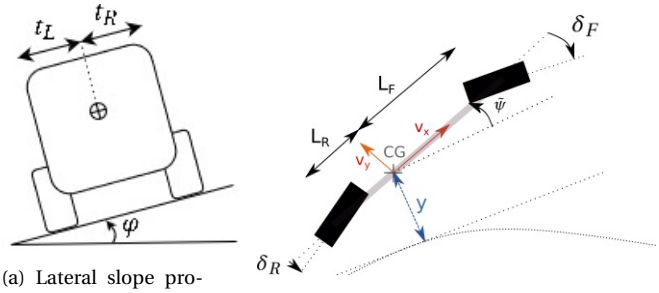
This work was supported by the French government through ANRT (Association Nationale Recherche Technologie) fundings.

Romain Legrand, Philippe Chevrel and Fabien Claveau are with IMT Atlantique, UBL, and also with the LS2N Laboratory, UMR CNRS 6004, 44000 Nantes, France (email : firstname.lastname@imt-atlantique.fr)

R. Legrand, B. Rancinangue and A. Dollet are with Secom Engineering, 44100 Nantes, France (email : brancinangue@secom.fr and adollet@secom.fr)

CG	Center of gravity
FL,FR	Index for the front left / right wheel
RL,RR	Index for the rear left / right wheel
$1SA$,$2SA$	Subscript relative to the situation with one steering axle / two steering axles
m	Vehicle total mass [kg]
I_z	Vehicle inertia w.r.t the vertical axis [kg.m^2]
L	Wheelbase of the vehicle [m]
t	Track width of the vehicle [m]
L_F,L_R	Distance of the CG to the front/rear axle [m]
t_L,t_R	Distance of the CG to the left /right track [m]
C_i	Cornering stiffness of the wheel i [N]
C_R	= C_{RL} + C_{RR} [N]
C_F	= C_{FL} + C_{FR} [N]
v_x,v_y	Longitudinal / Lateral vehicle speed, at the CG [m.s^{-1}]
a_x,a_y	Longitudinal / Lateral vehicle acceleration [m.s^{-2}]
$F_{y,i}$	Lateral forces applied on wheel i [N]
$\dot{\psi}$	Yaw speed of the vehicle [rad.s^{-1}]
δ_i	Steering angle of the wheel i [rad]
δ_F,δ_R	Mean steering angle of the front /rear axle [rad]
δ	= $\begin{pmatrix}\delta_F & \delta_R\end{pmatrix}^T$
δ_K/δ_{FF}	Steering angles' feedback / feedforward terms [rad]
ρ	Curvature of the reference trajectory [m^{-1}]
φ	Lateral slope angle [rad]
d	= $\begin{pmatrix}\rho & \sin(\varphi)\end{pmatrix}^T$
g	Acceleration of gravity [m.s^{-2}]
y	Lateral deviation w.r.t. the reference trajectory [m]
$\tilde{\psi}$	Angular deviation w.r.t. the reference trajectory [rad]
$\dot{\psi}$	Yaw rate [rad.s^{-1}]
x	= $\begin{pmatrix}\tilde{\psi} & \dot{\psi} & y & \dot{y}\end{pmatrix}^T$, state vector
X	= $\begin{pmatrix}\int\tilde{\psi} & \tilde{\psi} & \dot{\psi} & \int y & y & \dot{y}\end{pmatrix}^T$, augmented state vector
z	= $\begin{pmatrix}\tilde{\psi} & y\end{pmatrix}^T$
$T_{x\to y}$	Transfer function between the signal x (input) and y (output)
s	Laplace operator
w_u	Noise on the signal u (see Fig 2)
v_u	Input of the environment's generator model for the signal u (see Fig 2)

Table I: List of symbols and abbreviations



(a) Lateral slope projection

(b) Yaw projection

Fig. 1: Lateral slope and yaw projections

slopes of a possibly rugged terrain. This information can be used to estimate the speeds of all the wheels.

$$\begin{cases} v_{x,FL} = v_{x,RL} = v_x - t_L\dot{\psi} \simeq v_x \\ v_{x,FR} = v_{x,RR} = v_x + t_R\dot{\psi} \simeq v_x \\ v_{y,FL} = v_{y,FR} = v_y + L_F\dot{\psi} \\ v_{y,RL} = v_{y,RR} = v_y - L'_R\dot{\psi} \end{cases} \tag{1}$$

The longitudinal speeds are simplified according to the bicycle model's assumptions. The above expressions of the speeds at different points of the vehicle can be used to obtain an expression of the lateral forces on the wheels. Advanced models can compute these forces, such as the Pacejka/Dugoff models [17] or models tailored for agricultural purposes [18] which will be further used in the vehicle simulator. A linearized version, however, may be sufficient to provide behavioral trends and be used in the conceptual model, such as for the H_2/H_∞ control strategy. In this context, the forces may be considered proportional to the slip angle.

$$F_{y,i} = C_i\left(\delta_i - \text{atan2}\left(v_{yi}, v_{xi}\right)\right) \simeq C_i\left(\delta_i - \frac{v_{yi}}{v_{xi}}\right) \tag{2}$$

Using (1) and (2) on the fundamental principle of the dynamics on the lateral axis yields to (3).

$$\begin{aligned} ma_y &= F_{y,FL} + F_{y,FR} + F_{y,RL} + F_{y,RR} - mg\sin(\varphi) \\ &= \frac{-(C_F + C_R)v_y + (L_RC_R - L_FC_F)\dot{\psi}}{v_x} + \sum C_i\delta_i - mg\sin(\varphi) \end{aligned} \tag{3}$$

Equation (4) holds below, describing the evolution of the deviations regarding the reference trajectory [15]:

$$\begin{cases} \dot{y} = v_y + v_x\tilde{\psi} \\ \dot{\tilde{\psi}} = \dot{\psi} - v_x\rho \end{cases} \tag{4}$$

Because v_x is considered constant, that $a_y = \dot{v}_y + \dot{\psi}v_x$, and using (3) and (4) leads to:

$$\begin{aligned} \ddot{y} &= \frac{d}{dt}\left(v_y + v_x\tilde{\psi}\right) = \dot{v}_y + v_x\left(\dot{\psi} - v_x\rho\right) = a_y - v_x^2\rho \\ \ddot{y} &= \frac{-(C_F + C_R)}{mv_x}\dot{y} + \frac{C_F + C_R}{m}\tilde{\psi} + \frac{L'_RC_R - L'_FC_F}{mv_x}\dot{\psi} \\ &\quad - v_x^2\rho + \frac{1}{m}\sum C_i\delta_i - g\sin(\varphi) \end{aligned} \tag{5}$$

The same approach is used to obtain the yaw acceleration $\ddot{\psi}$ (6) through the principle of dynamics on the vertical axis (under the bicycle model assumption that $\delta_{FR} = \delta_{FL} = \delta_F$ and $\delta_{RL} = \delta_{RR} = \delta_R$)

$$\begin{aligned} I_z\ddot{\psi} &= L_F(F_{y,FL} + F_{y,FR}) - L_R(F_{y,RL} + F_{y,RR}) \\ \ddot{\psi} &= \frac{L_RC_R - L_FC_F}{I_zv_x}\dot{y} + \frac{L_FC_F - L_RC_R}{I_z}\tilde{\psi} \\ &\quad - \frac{L_F^2C_F + L_R^2C_R}{v_xI_z}\dot{\psi} + \frac{L_FC_F\delta_F - L_RC_R\delta_R}{I_z} \end{aligned} \tag{6}$$

By defining the state vector $x = \begin{pmatrix}\tilde{\psi} & \dot{\psi} & y & \dot{y}\end{pmatrix}^T$, vector $\delta = \begin{pmatrix}\delta_F & \delta_R\end{pmatrix}^T$ and exogenous inputs $d = \begin{pmatrix}\rho & \sin(\varphi)\end{pmatrix}^T$, the lateral model of the vehicle $\dot{x} = Ax + B\delta + Gd$ can be obtained by (4), (5) and (6). This extends the classic bicycle model by adding a second steering axle and by showing the lateral slope as an exogenous signal, which is less common.

$$A = \begin{pmatrix} 0 & 1 & 0 & 0 \\ \frac{L_F C_F - L_R C_R}{I_z} & -\frac{L_F^2 C_F + L_R^2 C_R}{I_z v_x} & 0 & \frac{L_R C_R - L_F C_F}{I_z v_x} \\ 0 & 0 & 0 & 1 \\ \frac{C_R + C_F}{m} & \frac{L_R C_R - L_F C_F}{m v_x} & 0 & -\frac{C_R + C_F}{m v_x} \end{pmatrix}$$

$$G = \begin{pmatrix} -v_x & 0 \\ 0 & 0 \\ 0 & 0 \\ -v_x^2 & -g \end{pmatrix}, \quad B = \begin{pmatrix} 0 & 0 \\ \frac{L_F C_F}{I_z} & -\frac{L_R C_R}{I_z} \\ 0 & 0 \\ \frac{C_F}{m} & \frac{C_R}{m} \end{pmatrix} \tag{7}$$

III. H_2/H_∞ MULTI-OBJECTIVE CONTROL DESIGN

A. Overall architecture and control objectives

The conception of the control law is presented in Fig. 2 below. First, a feedforward action (upper left in Fig. 2) is computed which takes advantage of the measurements of curvature and lateral slope angle associated with the reference trajectory. Second, an extended output feedback (bottom in Fig. 2) performs corrections on the steering commands, which is defined from gains applied to the output deviations and integrated deviations. The output deviation x_s is the difference between the current vehicle state x and the reference state associated with the reference path x_{FF} previously computed in the feedforward function. The exogenous signals considered to be disturbances include the curvature and lateral slope along the vehicle trajectory, and the models linked to these signals appear in the environment box and are detailed later.

The following control law is designed under the assumption that only 1SA or 2SA are available, which require separate control objectives. In the 1SA case, the control problem is to regulate the lateral deviation y, but when both steering actuators (δ_F and δ_R) are available, the control problem is to regulate both the lateral deviation y and the angular deviation $\tilde{\psi}$. This is because the simultaneous regulation of y and $\tilde{\psi}$ in the 1SA configuration is an unreachable objective [13].

Only the state vector x and environment variables d_m are measured in the control implementation. Disturbance signals such as w_δ, v_ρ, v_φ or w_d are only considered while computing the feedback gains (see Section III-E). While x and ρ_{mes} are measured relatively to the reference trajectory, φ_{mes} could be estimated via a Kalman filter as in [19].

B. 1SA and 2SA feedforward control design

The goal is to achieve a static inversion of the extended bicycle model by determining the steering angles δ_{FF} and the reference state x_{FF} in accordance with d_m, the measured signals associated with the environment. In static 1SA mode, the algebraic equations $0 = Ax_{FF} + B\delta_{FF} + Gd_m$ (see (7)) and $\delta_{R,FF} = 0$ hold. Defining the reference state by $y_{FF} = \dot{y}_{FF} = 0$ according to the control objectives enables inverting the system to obtain x_{FF} and δ_{FF} in (8).

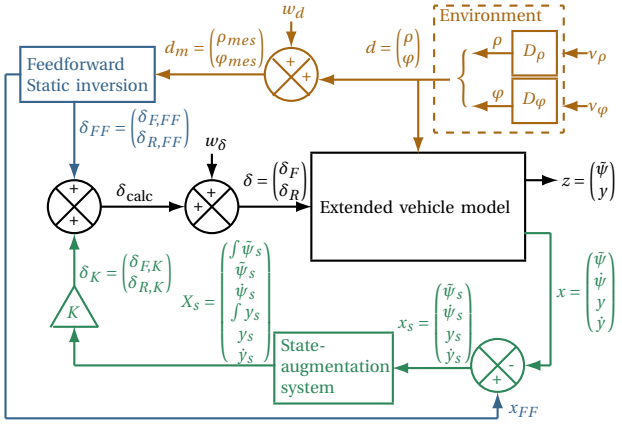


Fig. 2: Control architecture

$$0 = Ax_{FF} + B\delta_{FF} + Gd_m \Leftarrow \begin{cases} \delta_{FF} = F_{\delta,1SA} d_m \\ x_{FF} = F_{x,1SA} d_m \end{cases}$$

with

$$\begin{cases} F_{\delta,1SA} = \begin{pmatrix} L + m v_x^2 \frac{C_R L_R - C_F L_F}{C_F C_R L} & mg \frac{C_R L_R - C_F L_F}{C_F C_R L} \\ 0 & 0 \end{pmatrix} \\ F_{x,1SA} = \begin{pmatrix} -L_R + \frac{L_F m v_x^2}{L C_R} & v_x & 0 & 0 \\ \frac{mgL_F}{LC_R} & 0 & 0 & 0 \end{pmatrix}^T \end{cases} \tag{8}$$

It is similarly possible to invert the system in the 2SA case. The defined reference state could then be extended to $\dot{y}_{FF} = y_{FF} = \tilde{\psi}_{FF} = 0$, according to the control objectives, to achieve the feedforward control given by (9).

$$0 = Ax_{FF} + B\delta_{FF} + Gd_m \Leftarrow \begin{cases} \delta_{FF} = F_{\delta,2SA} d_m \\ x_{FF} = F_{x,2SA} d_m \end{cases}$$

with

$$F_{\delta,2SA} = \begin{pmatrix} L_F + \frac{L_R m v_x^2}{L C_F} & \frac{mgL_R}{LC_F} \\ -L_R + \frac{L_F m v_x^2}{L C_R} & \frac{mgL_F}{LC_R} \end{pmatrix}, \quad F_{x,2SA} = \begin{pmatrix} 0 & 0 \\ v_x & 0 \\ 0 & 0 \\ 0 & 0 \end{pmatrix} \tag{9}$$

It should be noted that $\dot{\psi}_{FF} = v_x \rho$ is not mentioned in the control objectives, and its value is obtained while solving the equation $0 = Ax_{FF} + B\delta_{FF} + Gd_m$.

C. 1SA and 2SA feedback control design

Once the determination of the feedforward components has been made, the feedback design must be considered, especially the pattern of the K matrix in Fig. 2. In the 1SA case, the control problem is to regulate the lateral deviation y (or both the lateral and angular deviation in the 2SA). Furthermore, in the 2SA case, this (2x6) feedback gain matrix K may be modified to consider different con-

figurations. Therefore, the three configurations considered in this paper are C1 : 1SA case; C2 : 2SA case with the front axle dedicated to the angular deviation, the rear axle to the lateral one; and C3 : 2SA case with full multivariable control. They are respectively associated with K as defined in (10).

$$\begin{cases} K_{C1} = \begin{pmatrix} 0 & k_{\tilde{\psi},F,1} & k_{\dot{\psi},F,1} & k_{\int y,F,1} & k_{y,F,1} & k_{\dot{y},F,1} \\ 0 & 0 & 0 & 0 & 0 & 0 \end{pmatrix} \\ K_{C2} = \begin{pmatrix} k_{\int \tilde{\psi},F,2} & k_{\tilde{\psi},F,2} & k_{\dot{\psi},F,2} & 0 & 0 & 0 \\ 0 & 0 & 0 & k_{\int y,R,2} & k_{y,R,2} & k_{\dot{y},R,2} \end{pmatrix} \\ K_{C3} = \begin{pmatrix} k_{\int \tilde{\psi},F,3} & k_{\tilde{\psi},F,3} & k_{\dot{\psi},F,3} & k_{\int y,F,3} & k_{y,F,3} & k_{\dot{y},F,3} \\ k_{\int \tilde{\psi},R,3} & k_{\tilde{\psi},R,3} & k_{\dot{\psi},R,3} & k_{\int y,R,3} & k_{y,R,3} & k_{\dot{y},R,3} \end{pmatrix} \end{cases} \tag{10}$$

Each gain of this generic feedback structure is then computed using an H_2/H_∞ multi-objective control synthesis (see Section III-E). This methodology allows defining performance objectives on the regulated variables while ensuring robustness, with the feedforward defined by (8) or (9) in the following section used, depending on the number of steering axles considered.

D. Generator models

a) Curvature: The dynamics of the reference curvature trajectory is modeled to consider its supposedly continuous and derivable character and to specify its probable evolution dynamic and variation domain. This information is valuable for formalizing and normalizing the optimization problem and for prediction purposes if necessary. The third-order model used (cf. (11)) is inspired by the one proposed in [20].

b) Lateral slope: : Similar arguments led to choosing a third-model generator model for the signal associated with the lateral slope. The maximum lateral slope angle considered is 0.38 rad, corresponding to a slope of 40%, which is a high but achievable value in vineyards.

$$\begin{cases} D_\rho(s) = \dfrac{\rho(s)}{\nu_\rho(s)} = \dfrac{\rho_{\max}}{(1+\tau_\rho s)\left(1+\dfrac{2\xi_\rho}{\omega_\rho}s+\dfrac{s^2}{\omega_\rho^2}\right)} \\ D_\varphi(s) = \dfrac{\varphi(s)}{\nu_\varphi(s)} = \dfrac{\varphi_{\max}}{(1+\tau_\varphi s)\left(1+\dfrac{2\xi_\varphi}{\omega_\varphi}s+\dfrac{s^2}{\omega_\varphi^2}\right)} \end{cases} \tag{11}$$

The impulse responses of the generator models are plotted in Fig. 3 and highlight the scenarios considered for the control synthesis, with the curvature ρ and lateral slope φ growing over a short period before returning to nominal values.

E. H_2/H_∞ optimization problem formulation

A H_2/H_∞ control problem is formalized to design a full- or sparse-gain matrix K, depending on the configuration considered in (10) in such a way that the system meets

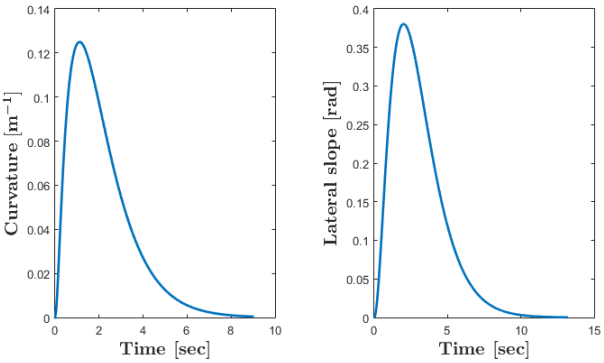


Fig. 3: Impulse responses of the curvature (left) and lateral slope (right) models

the control specifications.The objective function and constraints were elaborated to meet realistic specifications regarding performance and robustness. The objective function concerns performance (lowest influence of the curvature on the deviations,*i.e.* having the best path-following performances regarding the curvature). The optimization criteria (OC1) and (OC2) regard control robustness, while (OC3) and (OC4) concern performance despite ground slopes and measurement errors. Finally, (OC5) constrains the closed loop dynamics. The non-linearities of the actual system are ignored in (7) but are no longer overlooked by considering such robustness margins. Using the small gain theorem [21] and circle criterion [22] shows that robustness is acquired for certain classes of non-linearities such as those involved in the problem under consideration.

The considered multicriteria optimization problem (MOC) is defined hereafter (see Table I and Fig. 2 for notations), where the parameters γ_j ($j \in \{\text{module}, \text{dyn}, \varphi, d, \beta, \text{real}\}$) are chosen according to the control specifications (see Section IV-B for typical values).

MOC (Multicriteria optimization control) problem

$$\begin{aligned} &\text{minimize} && \left\| T_{\nu_\rho \to z} \right\|_2 \\ &\text{under constraints} && (OC1) : M_{\text{module}} = \frac{1}{\left\| T_{w_\delta \to \delta} \right\|_\infty} \geqslant \gamma_{\text{module}} \\ & && (OC2) : M_{\text{dyn}} = \frac{1}{\left\| s T_{w_\delta \to \delta_{\text{calc}}} \right\|_\infty} > \gamma_{\text{dyn}} \\ & && (OC3) : \left\| T_{\nu_\varphi \to z} \right\|_2 \leqslant \gamma_\varphi \\ & && (OC4) : \left\| T_{w_d \to z} \right\|_2 \leqslant \gamma_d \\ & && (OC5) : \text{Root locus} \begin{cases} -\text{damping } \gamma_\beta \\ -\text{real part } \gamma_{real} \end{cases} \end{aligned} \tag{MOC}$$

(OC1) represents the input sensitivity constraint to determine robustness regarding the actuators, in terms of modulus margin and circle criterion [22]. (OC2) is the high-frequency weighted complementary sensitivity constraint regarding the dynamic margin, which guarantees robustness against neglected dynamics at high frequencies and time delays ($\left\| s T_{w_\delta \to \delta_{\text{calc}}} \right\|_\infty^{-1}$ representing a time).

(OC3) ensures lower sensibilities of the regulation system to the lateral slope or to the measurement errors for (OC4). (OC5) is the closed-loop poles location constrained by γ_β and γ_{real} (Fig. 4).

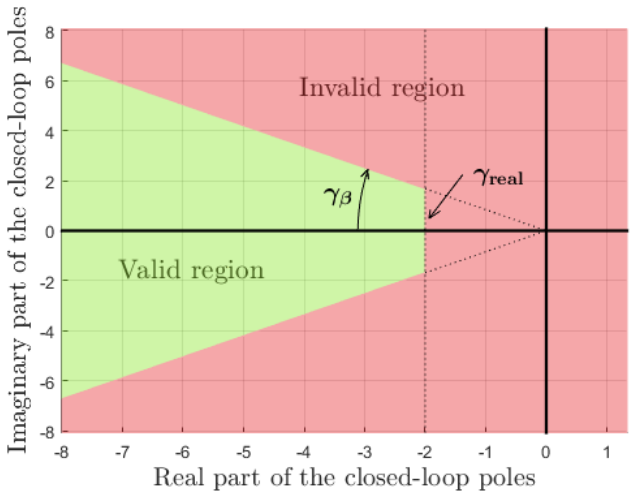


Fig. 4: Constrained location of the closed-loop poles

The optimized values of the feedback gains presented in (10) result from the solution of (MOC). To be as close as possible to specifications, no relaxation was used for convexification purposes. Following the example of [20], we used nonlinear and non-smooth optimization techniques [23], [24] to solve (MOC). Sub-gradients and a favorable initialization allow a rapid convergence of the parameters of the target control architecture, whereby we use the Systune solver (developed by MATLAB ®) [23], [25]. The longitudinal velocity of the vehicle is considered since it provides a measured time-varying parameter of the bicycle model. The adaptation to vehicle speed can be obtained using gain-scheduling [26], although it is not included in the scope of this paper. The simulation presented in the next section focuses on a constant longitudinal speed.

IV. Regulation results of lateral deviation and heading angle

A. Tests and simulator presentation

The simulator performed using MATLAB ®Simulink was designed by Secom Engineering. Relying on a 10-DOF dynamic model, it considers non-linear physical phenomena not described in the synthesis model, including the rolling resistance, the lateral and longitudinal slip forces on the four wheels using a wheel model tailored for agricultural purposes [18]; and the load transfers between all the wheels [27], depending on accelerations and slopes. The longitudinal and lateral dynamics are traditionally decoupled [28] but are coupled in the simulator. The steering actuation is also finely modeled, while the suspensions are not considered.

The scenario considered (Fig. 5) relevant for the agricultural sector is the following: On a slippery soil, we model an S trajectory (curvature of $1/8$ m^{-1}) on a sloping ground (10 deg or 18%) so that the vehicle remains canted in straight lines and descends during turns. The whole path is followed at a constant speed of 10 km/h, which enables testing the ability of the vehicle to counter lateral acceleration due to gravity in a straight line as well as its ability to follow a curved path as the slope changes to a downward slope.

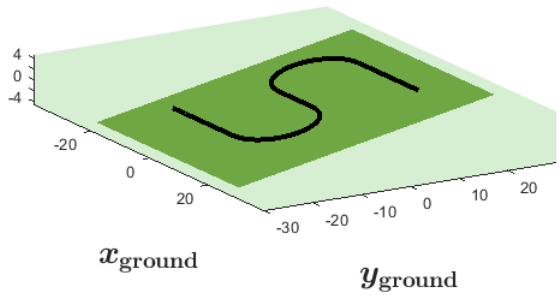


Fig. 5: Test trajectory on slope and slippery soil

The considered vehicle is a heavy off-road vehicle with the following characteristics (Table II):

L	3.21 [m]	Nominal C_F	307 [kN.rad^{-1}]
t	1.83 [m]	Nominal C_R	232 [kN.rad^{-1}]
h_{CG}	1.7 [m]	Mass m	6000 [kg]

Table II: Vehicle characteristics

B. Simulation results

a) Framework 1 - Comparison of the three configurations: Three configurations were defined in Section III-C : (C1), (C2) and (C3). Optimal gains are computed according to constraints (MOC) for each of these configurations using the following specifications : $\gamma_{\text{module}} = 0.2$, $\gamma_{\text{dyn}} = 0.5$, $\gamma_\varphi = 1$, $\gamma_d = 1$, $\gamma_\beta = 80°$ and $\gamma_{\text{real}} = -0.2$.

b) Framework 2 - Optimization of C3 configuration: Two steering angles enable seeking greater performance and robustness margins. This is especially necessary in complex situations with great changes in the vehicle's state and parameters. That is why more constraining parameters are considered : $\gamma_{\text{module}} = 0.9$, $\gamma_{\text{dyn}} = 0.7$, $\gamma_\varphi = 0.5$, $\gamma_d = 0.5$, $\gamma_\beta = 40°$ and $\gamma_{\text{real}} = -0.5$. These margins are too constraining for the C1 and C2 configurations according to the solver, hence their absence in this framework (see Table III).

c) Results of the multivariable control problem: As shown in Table III, the more gains contained in the K matrix, the greater the robustness of the whole control system. The comparison of the first three columns highlights that while the module and dynamic margins are close to specifications, the H_2 norms decrease as the number of

	Framework 1			Framework 2
	C1	C2	C3	C3
$\|T_{v_\rho \to z}\|_2$	0.126	0.0095	0.0043	7.9×10^{-3}
M_{module}	0.2001	0.3336	0.2738	0.9023
M_{dyn}	0.5002	0.5065	0.5013	0.7011
$\|T_{v_\varphi \to z}\|_2$	0.561	0.4417	0.238	5.74×10^{-5}
$\|T_{w_d \to z}\|_2$	0.9998	0.442	0.235	0.178

Table III: Results of the optimisation problem

non-zero gains in the K matrix (cf. (10)) increases. The configuration C3 shows great potential, as highlighted by favorable margins and H2 norms, even when using more binding constraints (cf. second framework).

d) : Results of the simulation

Fig. 6 presents the simulation results of the lateral and angular deviations for the three configurations in framework 1 (F1) and for the C3 configuration in framework 2 (F2).

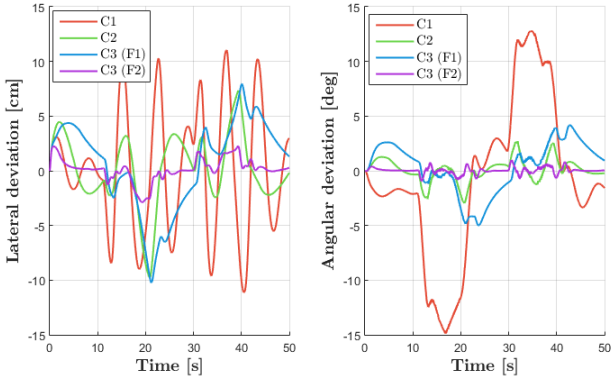


Fig. 6: Lateral (left) and angular (right) deviations

Concerning the 1SA situation, the angular deviation is sizeable, due to, for example, the control objective described in section III-C. Clear differences can be noticed between the three 2SA configurations in frameworks 1 and 2, with F2 being more effective, as suggested by table III. The second framework is more constraining and generated C3 gains ensuring better margins and performance as shown in Fig. 6 and revealing the potential of a well-tuned C3 configuration regarding adaptability to situations with significant slopes and slips. This highlights the importance of the parameters chosen in (MOC).

Fig. 7 presents the evolution of the steering angles in the 1SA (F1) and 2SA (F2) configurations.

For all situations, the steering angles applied to each vehicle are close to the feedforward term, except when the 2SA vehicle is in crab steering mode in straight lines. The steering angles are subject in this situation to a slight offset ($\simeq$ 1 deg) compared to the feedforward term, which seems to be too low to compensate the lateral slope. The turn performances, however, are satisfying for the 2SA vehicle

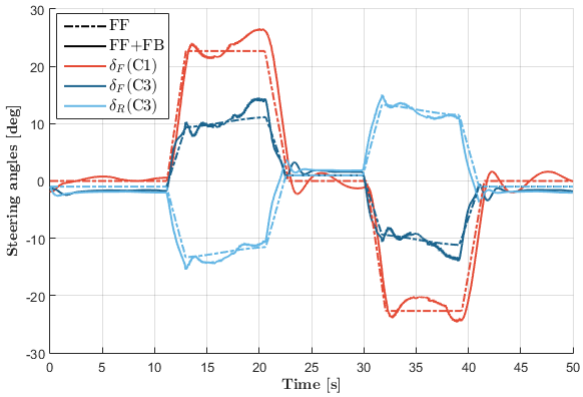


Fig. 7: Steering angles for a 1SA or 2SA situation

since the feedforward considers the changing slope, which is not visible in the 1SA vehicle.

V. Conclusions and Future Works

A. Conclusions

This paper presented a methodology to design a lateral control of a two-steering-axle off-road vehicle operating on slippery sloping grounds. It firstly extended the bicycle model to account for slope effects, which was used to design a lateral control for the considered class of vehicles that best utilizes the abilities of two-steering axles. The design methodology also enables designing without reformulating a control law for a one- or two-axle steering configuration, with a decentralized (decoupled PID) or centralized (multivariable) structure in the latter case. This leads to comparing the three solutions where, as expected, the multivariable controller of the two-axle steering achieved the best behavior. The considered control architecture effectively combines feedforward and feedback control. The methodology for the feedback part relies on an H_2/H_∞ synthesis. The performance, in terms of angular and lateral deviations regarding curvature and slopes, and the robustness were specified by H_2/H_∞ soft or hard constraints. Finally, a comparison was performed using a realistic non-linear simulator, leading to interesting conclusions regarding the design methodology and obtained controllers, namely the path-following abilities of two-steering-axle vehicles, which are useful in an off-road context (slippery soil, changing slopes). Furthermore, this resulting controller is simple to implement for vehicles and is consistent with a limited number of sensors. The computational load is also very low (small matrix multiplications and an integrator) for the embedded computer, the offline determination of the feedback gains being made offline.

B. Future works and perspectives

The methodology proposed in this article enables addressing the case of multiple steering axles with a wide range of geometric characteristics for the considered vehicle. These characteristics are the same as those needed

in the bicycle model. The research will be developed to further specify the sensitivity of the results to the uncertainties of key parameters such as the location of the potentially variable center of gravity and the tire characteristics.

REFERENCES

[1] W. G. Walter, "An imitation of life," *Scientific American*, vol. 182, no. 5, pp. 42–45. 1950.

[2] P. Daviet and M. Parent, "Longitudinal and lateral servoing of vehicles in a platoon," in *Proceedings of Conference on Intelligent Vehicles*, pp. 41–46, IEEE. 1996.

[3] T. Bell, "Precision robotic control of agricultural vehicles on realitic farm trajectories." PhD thesis, 1999.

[4] S. Mustaki, A.-T. Nguyen, P. Chevrel, M. Yagoubi, and F. Fauvel, "Comparison of two robust static output feedback h2 design approaches for car lateral control," in *2019 18th European Control Conference (ECC)*, pp. 716–723, IEEE. 2019.

[5] R. Attia, R. Orjuela, and M. Basset, "Coupled longitudinal and lateral control strategy improving lateral stability for autonomous vehicle," in *2012 American Control Conference (ACC)*, pp. 6509–6514, IEEE. 2012.

[6] F. Plestan, J. Davins-Valldaura, S. Moussaoui, and G. Pita-Gil, "Sliding mode observer design for the road curvature estimation in traffic jam pilot system," in *2016 14th International Workshop on Variable Structure Systems (VSS)*, pp. 302–307, IEEE. 2016.

[7] Y. Guo, H. Guo, Z. Yin, M. Cui, and H. Chen, "Vehicle lateral stability controller design for critical running conditions using NMPC based on vehicle dynamics safety envelope," in *2019 IEEE International Symposium on Circuits and Systems (ISCAS)*, pp. 1–8, IEEE. 2019.

[8] R. Lenain, B. Thuilot, O. Hach, and P. Martinet, "High-speed mobile robot control in off-road conditions: A multi-model based adaptive approach," in *2011 IEEE International Conference on Robotics and Automation*, pp. 6143–6149, IEEE. 2011.

[9] B. Fernandez, P. J. Herrera, and J. A. Cerrada, "A simplified optimal path following controller for an agricultural skid-steering robot," *IEEE Access*, vol. 7, pp. 95932–95940. 2019.

[10] M. Deremetz, "Contribution à la modélisation et à la commande de robots mobiles autonomes et adaptables en milieux naturels." PhD thesis, 2018.

[11] L. Saleh, P. Chevrel, F. Mars, J.-F. Lafay, and F. Claveau, "Human-like cybernetic driver model for lane keeping," *IFAC Proceedings Volumes*, vol. 44, no. 1, pp. 4368–4373. 2011.

[12] M. Deremetz, R. Lenain, A. Couvent, C. Cariou, and B. Thuilot, "Path tracking of a four-wheel steering mobile robot: A robust off-road parallel steering strategy," p. 7. 2017.

[13] R. Rajamani, *Vehicle dynamics and control*. Mechanical engineering series, Springer, 2. ed ed. 2012.

[14] M. Richier, R. Lenain, B. Thuilot, and C. Debain, "Dual backstepping observer to anticipate the rollover risk in under/over-steering situations. application to ATVs in off-road context," in *2012 IEEE/RSJ International Conference on Intelligent Robots and Systems*, pp. 5387–5393, IEEE. 2012.

[15] S. E. Mustaki, "Outils de pré-calibration numérique des lois de commande de systèmes de systèmes: application aux aides à la conduite et au véhicule autonome." PhD thesis, 2019.

[16] L. Menhour and D. Koenig, "Simple discrete-time switched h optimal control: Application for lateral vehicle control," in *1st IFAC Workshop on Linear Parameter Varying Systems (LPVS 2015) Grenoble, France*. 2015.

[17] E. Bakker, L. Nyborg, and H. B. Pacejka, "Tyre modelling for use in vehicle dynamics studies," in *SAE International Congress and Exposition*. 1987.

[18] W. Hirschberg, G. Rill, and H. Weinfurter, "User-appropriate tyre-modelling for vehicle dynamics in standard and limit situations," *Vehicle System Dynamics*, vol. 38, no. 2, pp. 103–125. 2003.

[19] B. L. Boada, D. Garcia-Pozuelo, M. J. L. Boada, and V. Diaz, "A constrained dual kalman filter based on pdf truncation for estimation of vehicle parameters and road bank angle: Analysis and experimental validation," *IEEE Transactions on Intelligent Transportation Systems*, vol. 18, no. 4, pp. 1006–1016, 2017.

[20] S. Mustaki, P. Chevrel, M. Yagoubi, and F. Fauvel, "Efficient multi-objective and multi-scenarios control synthesis methodology for designing a car lane centering assistance system," in *2018 European Control Conference (ECC)*, pp. 929–934, IEEE. 2018.

[21] G. Zames, "Input-output feedback stability and robustness," *IEEE Control Systems Magazine*, vol. 16, no. 3, pp. 61–66, 1996.

[22] M. Arcak and P. Kokotović, "Feasibility conditions for circle criterion designs," *Systems & Control Letters*, vol. 42, no. 5, pp. 405–412, 2001.

[23] P. Apkarian, P. Gahinet, and C. Buhr, "Multi-model, multi-objective tuning of fixed-structure controllers," *(ECC). IEEE Publ. Piscataway, NJ*, vol. 42, pp. 856–861. 2014.

[24] P. Apkarian and D. Noll, "Optimization-Based Control Design Techniques and Tools," in *Encyclopedia of Systems and Control*, 2015.

[25] M. S. Sadabadi and D. Peaucelle, "From static output feedback to structured robust static output feedback: A survey," *Annual Reviews in Control*, vol. 42, pp. 11–26. 2016.

[26] X. Huang, H. Zhang, G. Zhang, and J. Wang, "Robust weighted gain-scheduling h_∞ vehicle lateral motion control with considerations of steering system backlash-type hysteresis," *IEEE Transactions on Control Systems Technology*, vol. 22, no. 5, pp. 1740–1753, 2014.

[27] Z. Shuai, H. Zhang, J. Wang, J. Li, and M. Ouyang, "Lateral motion control for four-wheel-independent-drive electric vehicles using optimal torque allocation and dynamic message priority scheduling," *Control Engineering Practice*, vol. 24, pp. 55–66. 2014.

[28] R. N. Jazar, *Vehicle dynamics: theory and applications*. Springer, corrected at 3. printing ed. 2009.